JTTEE5 15:518-523
DOI: 10.1361/105996306X146866
1059-9630/$19.00 © ASM International

Peer Reviewed

Numerical Simulation of the Cold Gas Dynamic Spray Process

M. Karimi, A. Fartaj, G. Rankin, D. Vanderzwet, W. Birtch, and J. Villafuerte

(Submitted February 27, 2006; in revised form April 4, 2006)

A computational fluid dynamic (CFD) model of the cold gas dynamic spray process is presented. The gas dynamic flow field and particle trajectories within an oval-shaped supersonic nozzle as well as in the immediate surroundings of the nozzle exit, before and after the impact with the target plane, are simulated. Predicted nozzle wall pressure values compare well with experimental data. In addition, predicted particle velocity results at the nozzle exit are in qualitative agreement with those obtained using a side-scatter laser Doppler anemometer (LDA). Details of the pattern of the particle release into the surroundings are visualized in a convenient manner.

Keywords cold gas dynamic spraying, modeling, particle dispersion pattern, particle-substrate impact, spray deposition

1. Introduction

The cold gas dynamic spray (CGDS) process is a relatively new material deposition technique with many advantages over the more conventional methods. It is a direct material deposition process that utilizes the kinetic energy of particles sprayed at very high velocities to produce bonding of the particles to a target. The method was originally developed at the Institute of Theoretical and Applied Mechanics of the Russian Academy of Science in Novosibirsk (Ref 1). The idea originated in the mid-1980s accidentally while studying particle erosion of a target surface. Instead of erosion, rapidly increasing deposition occurred as particles hit the target faster than a threshold velocity, called the critical velocity (Ref 2). The idea culminated in the granting of U.S. and European patents in the middle 1990s (Ref 3, 4).

In this technique, particles are accelerated to very high speeds by means of a carrier gas forced through a converging-diverging de Laval nozzle. Two different approaches can be adopted to introduce the particles to the gas stream. In the first approach, the particles are introduced before the nozzle, where the gas pressure is essentially higher than the ambient pressure (Ref 3, 4). In this approach, referred to as Papyrin's process, the powder particles must be pushed at high pressure into the stream. In the second approach, however, particles are introduced downstream of the nozzle throat (Ref 5). In this case, the gas supply pressure can be carefully chosen such that the pressure of the particle feed would be lower than the ambient pressure and the powder particles along with some airflow are drawn in by the stream vacuum pressure.

The process does not have a 100% deposition rate; therefore, particles can bounce off the target and escape into the working environment. Depending on the material and size distribution of the sprayed particles, this can cause health and safety hazards

This article was originally published in *Building on 100 Years of Success, Proceedings of the 2006 International Thermal Spray Conference* (Seattle, WA), May 15-18, 2006, B.R. Marple, M.M. Hyland, Y.-Ch. Lau, R.S. Lima, and J. Voyer, Ed., ASM International, Materials Park, OH, 2006.

M. Karimi, Centerline (Windsor) Ltd., SST Division; University of Windsor, Mechanical, Automotive and Materials Engineering; **A. Fartaj** and **G. Rankin,** University of Windsor, Mechanical, Automotive and Materials Engineering; **D. Vanderzwet** and **W. Birtch,** CenterLine (Windsor) Ltd., SST Division; and **J. Villafuerte,** CenterLine (Windsor) Ltd. Contact e-mail: mo.karimi@gmail.com.

Nomenclature

C_D	drag coefficient
d	diameter
e	coefficient of restitution
h	convective heat transfer coefficient
l	standoff distance
M	Mach number
M	rotational mechanical impulse
Nu	Nusselt number
p	pressure
P	linear mechanical impulse
Re	Reynolds number
t	maximum nozzle thickness
T	temperature
w	domain semiwidth
y	target center to boundary clearance
z	distance from nozzle throat along nozzle axis
θ	angle between nozzle axis and target normal
*	nozzle throat

Subscripts

e	nozzle exit
f	particle feed
n	normal component of vector
o	stagnation
p	particle
t	tangential component of vector

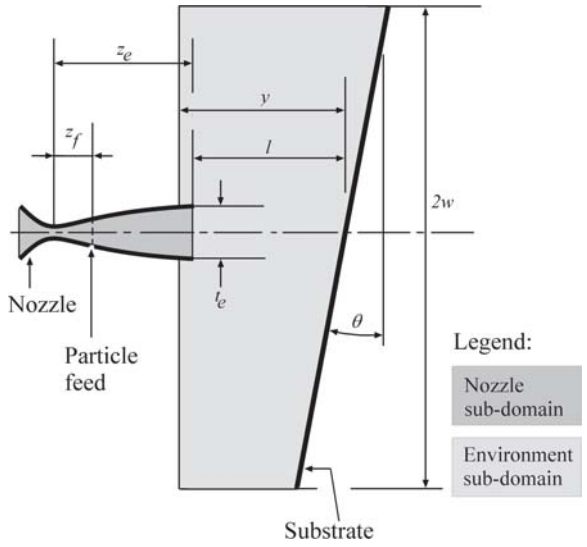

Fig. 1 Calculation domain for the simulation (not to scale)

(Ref 6, 7). To minimize possible risks, the current practice is to place the process equipment and workpiece in a large stationary enclosure. It would be desirable to have a portable exhaust collection facility so that the process can be conducted in a normal shop environment.

The ability to design a capture-at-source particle exhaust system to collect the rebounding particles requires the knowledge of the flow field and particle trajectories in the process. The objective of this research is to develop the necessary tools and a procedure to be used with an available commercial software package and to conduct a numerical investigation of the gas/particle flow field inside the nozzle and within the surroundings of an idealized target to model the CGDS process. The numerical model is partially validated using available experimental data. The locations and concentrations of particles leaving the boundaries of a domain of interest are predicted and presented in a graphical manner that is easy to interpret.

2. Numerical Methodology

To perform the simulation, FLUENT 6.2 (Fluent Inc., Lebanon, NH) is used. The calculation domain of particular interest is shown schematically in Fig. 1. Values of 2 cm for y and 2.5 cm for w, which define the extent of the calculation domain, were found to be large enough to capture all important features of the flow and accurately describe the distribution of particles leaving the enclosure. In addition, the boundaries are far enough away so as not to affect the solution of the flow field.

The nozzle has a round cross section up to the particle feed location with a throat diameter, d^*, of 2.66 mm. This round shape transforms to an oval shape in a diverging tube stretched from downstream of the particle feed to the nozzle exit. This tube, known as nozzle tube, is approximately 12 cm long. The dimensions of the nozzle cross section at its exit plane, t_e has values of 9.0 and 6.0 mm along the major and minor axes, respectively. The distances of the nozzle exit and particle feed from nozzle throat, z_e and z_f, are 13.9 cm and 5.6 mm, respectively.

The gas flow in the nozzle is supersonic for some distance downstream of the throat, but becomes subsonic due to an oblique shock wave inside the nozzle. The flow velocity at the nozzle exit, however, is high enough so that the coupling of the nozzle flow field with the outside environment is weak and separation of the flow field into two subdomains, nozzle and environment, is a reasonable approximation. This approximation allows the use of the same nozzle flow to simulate the environment with the large number of combinations of standoff distances and nozzle-target angles that are studied using this method. The entire set of results is too large to include in this paper. The nozzle alone (disregarding the environment) has two longitudinal planes of symmetry, making it feasible to reduce the model to a one-quarter model. Eliminating the need to resolve the nozzle flow field for each substrate condition as well as taking advantage of the additional plane of symmetry in the nozzle greatly reduced the overall project computational time. The nozzle and the environment subdomains are shown in Fig. 1.

2.1 Flow Field

A structured scheme is used to create hexahedral elements throughout the field, except adjacent to the nozzle axis where wedge elements are required. The mesh consists of 29,760 cells for the nozzle subdomain and, depending on the standoff distance, l, and the target tilting angle, θ, between 53,166 and 94,042 for the environment subdomain. The independence of the solution to the grid size is ensured through a grid dependency study for the flow field of the nozzle as well as one typical geometry of the environment (Ref 8).

The ideal-gas law is used to account for compressibility effects along with the continuity, momentum, and energy equations. To model the turbulence, a modification to the k-ε model is used that accounts for compressibility effects. This was proposed and successfully applied by Sarkar et al. (Ref 9, 10). In addition, the temperature dependence of the viscosity is accounted for using the Sutherland law (suited for high-speed compressible flows, Ref 11). The coupled-implicit solver with a second-order discretization scheme is suitable for this study (Ref 11, 12).

2.2 Particle-Fluid Interaction

To obtain the particle trajectories, the Discrete Phase toolbox of FLUENT is used to simulate the trajectories of particles in a Lagrangian frame of reference. This formulation assumes that the second phase is sufficiently dilute so that particle-particle interactions and the effects of the particle volume fraction on the gas phase can be neglected. These facts impose the condition that the discrete phase must be present at low volume fractions. Enough evidence is available to support this condition (Ref 2, 13-15).

The nozzle model consists of one quarter of the nozzle, whereas the particle trajectories are not symmetric because the particle feed location is not symmetric. A new method is used to perform asymmetric particle trajectory calculation within a symmetric flow field (Ref 8).

2.2.1 Drag Coefficient. The particle motion is caused by the drag force exerted on the particles by the flow field. The magnitude of this force depends on the drag coefficient, C_D. The

analysis of this coefficient focuses on the fluid-particle interaction; therefore, the Reynolds and Mach numbers, Re_p and M_p, should be determined corresponding to the relative movement of the fluid with respect to the particles. A correlation was proposed in 1978 by Clift et al. (Ref 16) that accounts for a wide range of flow-particle Mach numbers and Reynolds numbers ($0.1 < M_p < 10$ and $0.2 < Re_p < 10^4$). This range accommodates the conditions encountered in CGDS applications. The effect of particle and gas temperatures, as well as the specific heat ratio of the gas is also taken into account. No correlations could be found to include the effects of the particle shape and compressibility simultaneously.

2.2.2 Turbulence. The stochastic nature of turbulence introduces uncertainties that affect particle trajectories. A stochastic tracking technique that utilizes an estimate of the instantaneous fluid velocity along the path of integration is used to model the turbulent dispersion of the particles. Details of this method are described in the literature (Ref 11).

2.2.3 Heat Transfer. Heat transfer between the particles and the carrier gas is important as the critical velocity of a particle depends on its temperature at the time of impact (Ref 17). For internal heat transfer of particles, it is assumed that there is negligible internal resistance to heat transfer (previously used by Stoltenhoff et al., Ref 18). All thermodynamic properties of the heat transfer process are constant, except for the flow-particle convective heat transfer coefficient, h_p. This coefficient appears in the definition of the flow-particle Nusselt number, Nu_p (the nondimensional ratio of convective to conductive heat transfer). In this study, a correlation is used to evaluate Nu_p that has been shown to accurately predict the temperature values (Ref 8).

2.3 Particle-Wall Interaction

In a CGDS system, when a particle hits the target, it either sticks or bounces off. This process is of a statistical nature and depends on many parameters such as the kinetic energy of the particle, its shape, the angle of attack, and so forth. However, as a simplifying assumption, to determine which case occurs, the normal component of the impact velocity is compared with the critical velocity.

For the case of rebound, the equations of impact dynamics must be considered to determine the normal and tangential components of the particle velocity after impact. The equations for a sphere traveling on a plane perpendicular to the target plane reduce to the normal, tangential, and angular momentum equations, that is, P_n, P_t, and M, respectively (Ref 19). Although the numerical technique does not consider any angular velocity for a particle, the angular momentum equations are still considered in the impact analysis. At each impact, however, the initial angular velocity of a particle is assumed to be zero, and its updated value is discarded after the impact calculations are completed.

Upon impact, the particle begins sliding on the surface. Depending on the conditions of impact, two different scenarios can occur. In the first scenario, the particle keeps sliding throughout the impact, whereas in the second scenario, the particle stops sliding during the impact and keeps rolling for the rest of the contact duration. With the particle size range encountered in CGDS applications (1 to ~100 μm), an analysis of impact conditions shows that the second scenario always occurs (Ref 8). The equations of impact dynamics in this case are simplified such that a constant value of 5/7 is obtained for the tangential coefficient of restitution, e_t. In this case, this value is the ratio of the tangential component of the particle velocity after the impact to that before the impact.

Kleis and Hussainova (Ref 20) proposed a procedure for estimating the normal coefficient of restitution, e_n. In this procedure, the values of the dynamic hardness as well as the elastic deformation of the particle at one arbitrary velocity are required. A revised form of this procedure was developed for use where, instead of these two parameters, the critical velocity under the impact conditions and the normal coefficient of restitution at an arbitrary velocity are required (Ref 8). The critical velocity values of different materials are available in the literature (Ref 2-4, 21-23). For the normal coefficient of restitution at an arbitrary velocity, a value between 0.07 and 0.10 is assumed at a velocity slightly below the critical velocity (as much as 20 m/s). This assumption agrees well with the impact conditions whose parameters are well known. The same technique is used to account for particle-wall interactions that occur both inside the nozzle and on the impact target.

2.4 Boundary and Initial Conditions

2.4.1 Flow Field. For the nozzle subdomain, a pressure inlet is used as the boundary condition at the nozzle inlet. The direction of the velocity vector is assumed to be perpendicular to this boundary. A turbulence intensity of 1% and a length scale equal to 20% of the nozzle diameter are used and have been previously shown to be accurate for similar flow fields (Ref 24). The pressure and temperature are obtained using a pressure gage connected to a wall pressure tap and a thermocouple at a location upstream of the throat where the velocity is very low. These values are very close approximations to the total pressure, p_o, and the total temperature, T_o, entering the nozzle. The total temperature is the temperature obtained by decelerating the flow to zero velocity in an adiabatic manner, while the total pressure is the pressure obtained by decelerating the flow to zero velocity in an isentropic manner.

The nozzle outlet is a pressure outlet, with the static pressure equal to the atmospheric pressure as is the case at the exit of a subsonic jet. This is in agreement with experimental results presented in section 3.1.2. The direction of the velocity vector is obtained from neighboring cells in this region. Heat transfer between the fluid and the nozzle walls is assumed to have an insignificant effect on the solution of the nozzle subdomain and, hence, all walls are considered to be adiabatic.

For the environment subdomain, the nozzle outlet, which is the inlet to this subdomain, is also set to a pressure inlet. The flow field values at this boundary are taken from the solutions from the nozzle subdomain. The methodology and tools developed to perform this task are discussed later.

The surrounding boundaries of the environment subdomain are pressure outlets, with pressure equal to the atmospheric pressure. The direction of the velocity vector is obtained from neighboring cells in these regions. Finally, the wall boundary conditions are treated in a similar manner to those in the nozzle subdomain.

2.4.2 Particle Tracking. In the nozzle subdomain, the flow domain contains the particle feed section of the nozzle. The projection of the cross section of the particle feed tube (at an

angle of 45° with the nozzle tube) on the nozzle cross section forms an ellipse. Therefore, in the numerical model, particles are inserted on this ellipse and randomly distributed over it. The distribution implies that the particles are more likely to appear closer to the center of the particle feed tube than at its periphery. This is accomplished by more heavily weighing the random number near the center. The velocity vector must be randomly chosen from a range of acceptable variations. These variations are selected based on the geometry of the particle feed. They are tuned such that an acceptable agreement with the experimental results in velocity predictions is achieved. Experimentally, it is not possible to determine a size distribution for the particles over the size range considered. Therefore, it is assumed that the size distribution of the particles is uniform.

For the environment subdomain, particles are initiated at the nozzle outlet so that the trajectory calculations can continue from where they terminated in the nozzle solution. To achieve this, all of the particle data must be taken from the nozzle solution at the nozzle outlet. At this point, the data can be compared with experiments and modifications, if needed, can be performed on the velocity magnitudes. The methodology and tools developed to perform these tasks are discussed later.

2.4.3 Transfer of Data between the Two Subdomains. The two solution subdomains are connected through the nozzle outlet. These solution subdomains are linked by fitting a curve to the values of each of the field variables in terms of the coordinates. A MATLAB (The MathWorks Inc., Natick, MA) code has been generated to fit a thin-plate smoothing spline (Ref 25) to the data points corresponding to each of the field variables obtained from the nozzle solution. The value of each of the flow field variables is then estimated at the cell centers of the environment solution using the generated curve.

For transferring the particle data, the CFD software package provides a tool that allows for recording into a file all the characteristic data regarding all particles as they hit or pass through a certain surface. Using this tool in the nozzle subdomain, a file is generated that serves as a data source to initiate the particles in the environment subdomain. Any modification to the particle velocities based on the comparison with experimental results is performed at this point.

3. Results

Results are presented for aluminum particles at an upstream temperature and a pressure of 300 °C and 500 kPa, respectively.

3.1 Nozzle Subdomain

3.1.1 Particle Trajectory Results. Particle velocities at the nozzle exit plane are presented in Fig. 2. The contour shown in this plot is fitted to the velocity data pertaining to 2500 particles using MATLAB. This contour is strongly asymmetric along the major axis and relatively uniform along the minor axis.

The oval shape of the nozzle is represented by an ellipse located at the bottom of the space. Each magenta dot located inside this ellipse represents a particle leaving the nozzle outlet. It can be seen that the particle distribution is considerably asymmetric about the major axis, but relatively symmetric about the minor axis. This is caused by the orientation of the particle feed. The

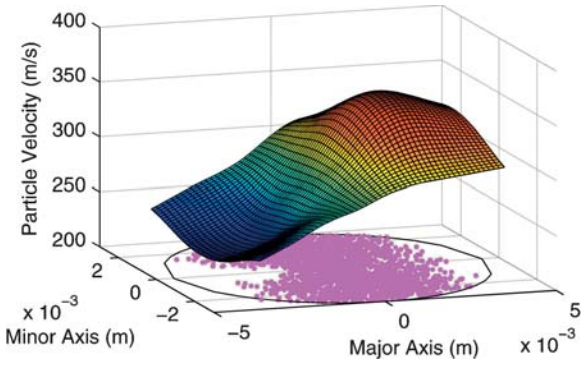

Fig. 2 Numerically obtained contour of particle velocities at the nozzle exit plane

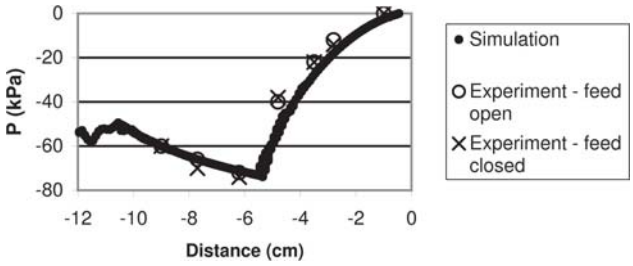

Fig. 3 Comparison of experimental and numerical values for the pressure at the tube wall

particles enter the nozzle at the negative side of the major axis. The simulation results show that when passing through the nozzle most particles hit the walls at the positive and then negative side of the walls consecutively. The experimental wear pattern on the nozzle sides supports this finding. Upon leaving the nozzle, the particle concentration is slightly higher toward the positive side of the major axis.

3.1.2 Validation of the Nozzle Static Pressure. Wall pressure values along the nozzle tube are shown in Fig. 3. It can be observed that the simulation results agree very well with the actual pressure values. Pressure values for the two cases of the particle feed being opened or closed are also very similar (differences are not larger than the resolution of the pressure gage used, i.e., 2 kPa). This confirms that neglecting the particle feed airflow in the simulation will not significantly affect the final results. The abrupt change in pressure that is evident at a distance of approximately −6 cm indicates that the flow undergoes an oblique shock wave inside the nozzle. This is not favorable because the flow velocity significantly drops beyond this shock wave, resulting in a subsonic flow at the nozzle outlet.

3.1.3 Validation of the Particle Velocities. A comparison of the simulation results with the experiment is shown in Fig. 4. The simulation profiles are extracted from the contour fitted to the particle velocities, as mentioned previously. The trends in the predicted profiles along both axes agree very well with the experimental results. The predicted particle velocities, however, are 15% lower than the values obtained experimentally. For the simulation of the environment subdomain, a modified value of the velocity is used. This is simply an increase, by 15%, in the longitudinal particle velocities and was incorporated to avoid including this discrepancy in the environment calculation.

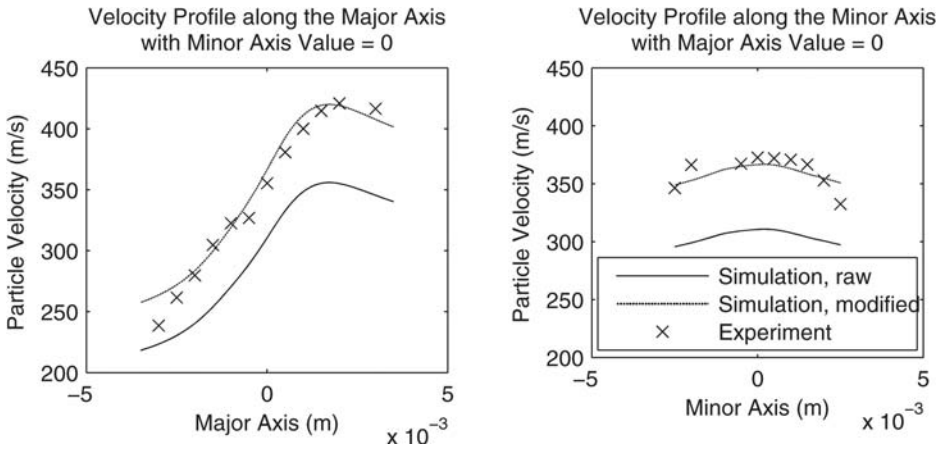

Fig. 4 Particle velocity profiles at the nozzle exit plane, simulation versus experimental results

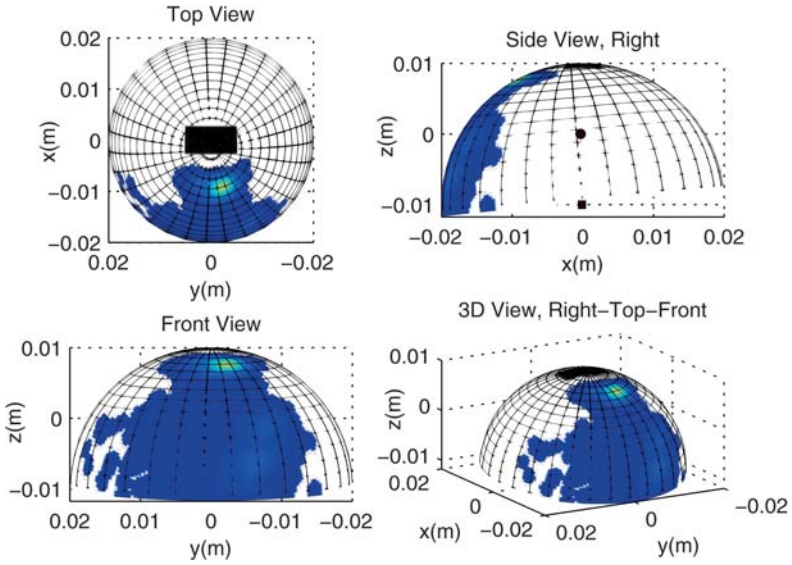

Fig. 5 Concentration of particles entering the surrounding

A number of factors could cause the discrepancy in the measured and predicted particle velocity magnitudes. The use of the spherical drag law approximation would result in drag coefficients lower than those present in reality. Inaccuracies of the model used to simulate the manner in which the particles enter the nozzle as well as inexactness of the impact model could be other reasons for this discrepancy.

3.2 Environment Subdomain

A preliminary study of a typical case revealed that 7000 particles is a statistically large sample, and therefore this sample size was used in the following procedure. The trajectories are available as a FLUENT output file, giving all particle properties at each time step. A C-language code along with a MATLAB code were developed to postprocess this file and generate the particle concentration contours on the surface of a hemisphere. The hemispherical shape allows comparison of the particle concentration at equal distances from the source, regardless of the direction of the particle motion. In this representation, the white regions are absolutely clean (no particle is passing through), whereas even one particle passing through a region will result in a small dark blue zone.

The image corresponding to the case of a standoff distance of $l = 10$ mm, and a target tilting angle of $\theta = 5°$, is shown in Fig. 5. The hemisphere shown is centered at the intersection of the nozzle centerline and the target plane. The center of the nozzle exit plane is located on the z axis of the coordinate system at a value of 0 as indicated by a solid dot in the "Side View, Right" image of Fig. 5. The center of the target plane is located at a z value of −0.01 m, as indicated by a solid square in the view, giving a standoff distance of 0.01 m. The radius of the hemisphere is 2 cm. The black rectangle located on top represents the location where the nozzle intersects this imaginary surface. The fact that this rectangle is not concentric with respect to the pole of the sphere, evident in the top view, clearly indicates that the target plate is tilted at a particular angle.

It is evident that most particles leave the hemisphere surface through a band extending from the side of the nozzle to the target. Within this band, the concentration is significantly higher close to the nozzle side, forming a bright spot in that area. For these operating conditions, the direction toward which the target is tilted mainly determines the location of the particles after rebounding from the target. The band of high concentration itself is not symmetric about the nozzle plane of symmetry. This is due to the asymmetry in the location of the particle feed.

4. Summary and Conclusions

The CFD tool that has been developed was successfully used to perform the required simulation. It should be emphasized that this technique is general enough to be applied, sometimes with minor modifications, to various combinations of geometrical and operational parameters. The flow field calculation is validated by comparison with wall pressure measurements and is in very good agreement. The numerically obtained particle velocities at the nozzle outlet demonstrate similar trends as the experimental results obtained using the LDA method. The velocity magnitudes, however, are underestimated. A method is developed for postprocessing the data that is convenient for providing qualitative comparisons.

Acknowledgments

The project was mainly funded and supported by CenterLine (Windsor) Ltd. (Windsor, Ontario, Canada) and partially supported through Discovery Grants from the Natural Sciences and Engineering Research Council of Canada (Grant Numbers: OGP0001403 and OGP0105727).

References

1. A.P. Alkhimov, V.F. Kosareve, and A.N. Papyrin, A Method of Cold Gas-Dynamic Spray Deposition, *Dokl. Akad. Nauk SSSR,* 1990, **315**(5), p 1062-1065, in Russian
2. R.C. Dykhuizen and M.F. Smith, Gas Dynamic Principles of Cold Spray, *J. Therm. Spray. Technol.,* 1998, **7**(2), p 205-212
3. A.P. Alkhimov, A.N. Papyrin, V.F. Kosarev, N.I. Nesterovich, and M.M. Shushapanov, "Gas-Dynamic Spray Method for Applying a Coating," U.S. Patent 5,302,414, 1994
4. A.P. Alkhimov, A.N. Papyrin, V.F. Kosarev, N.I. Nesterovich, and M.M. Shushapanov, "Method and Device for Coating," European Patent 0 484 533 B1, 1995
5. A.I. Kashirin, O.F. Klyuev, and T.V. Buzdygar, "Apparatus for Gas-Dynamic Coating," U.S. Patent 6,402,050, 2002
6. M. Cowley, Dusting-Off the Hazards of Powder Coating, *Finishing,* 2003, **27**(12), p 18-21
7. H. Heriaud-Kraemer, G. Montavon, S. Hertert, H. Robin, and C. Coddet, Harmful Risks for Workers in Thermal Spraying: A Review Completed by a Survey in French Company, *J. Therm. Spray. Technol.,* 2003, **12**(4), p 542-554
8. M. Karimi, "An Investigation of the Cold Gas Dynamic Supersonic Spray Process Particle/Flow Field," M.A.Sc. thesis, University of Windsor, 2005
9. S. Sarkar, G. Erlebacher, M.Y. Hussaini, and H.O. Kreiss, Analysis and Modelling of Dilatational Terms in Compressible Turbulence, *J. Fluid Mech.,* 1991, June, **227**, p 473-493
10. S. Sarkar and B. Lakshmanan, Application of a Reynolds Stress Turbulence Model to the Compressible Shear Layer, *AIAA J.,* 1991, **29**(5), p 743-749
11. Fluent 6.2 User's Guide, Fluent Inc., Lebanon, NH, 2005
12. B. Jodoin, Cold Spray Nozzle Mach Number Limitation, *J. Therm. Spray. Technol.,* 2002, **11**(4), p 496-507
13. M. Grujicic, C. Tong, W.S. DeRosset, and D. Helfritch, Flow Analysis and Nozzle-Shape Optimization for the Cold-Gas Dynamic-Spray Process, *Proc. Inst. Mech. Eng., Part B: J. Eng. Manuf.,* 2003, **217**(11), p 1603-1613
14. V. Shukla, G.S. Elliott, and B.H. Kear, Nanopowder Deposition by Supersonic Rectangular Jet Impingement, *J. Therm. Spray. Technol.,* 2000, **9**(3), p 394-398
15. P.H. Shipway and I.M. Hutchings, Method for Optimizing the Particle Flux in Erosion Testing with a Gas-Blast Apparatus, *Wear,* 1994, **174** (1-2), p 169-175
16. R. Clift, J.R. Grace, and M.E. Weber, *Bubbles, Drops, and Particles,* Academic Press, New York, 1978
17. V.F. Kosarev, S.V. Klinkov, A.P. Alkhimov, and A.N. Papyrin, On Some Aspects of Gas Dynamics of the Cold Spray Process, *J. Therm. Spray. Technol.,* 2003, **12**(2), p 265-281
18. T. Stoltenhoff, H. Kreye, and H.J. Richter, An Analysis of the Cold Spray Process and Its Coatings, *J. Therm. Spray. Technol.,* 2002, **11**(4), p 542-550
19. R.M. Brach, Impact Dynamics with Applications to Solid Particle Erosion, *Int. J. Impact Eng.,* 1988, **7**(1), p 37-53
20. I. Kleis and I. Hussainova, Investigation of Particle-Wall Impact Process, *Wear,* 1999, **233-235,** p 168-173
21. D.L. Gilmore, R.C. Dykhuizen, R.A. Neiser, T.J. Roemer, and M.F. Smith, Particle Velocity and Deposition Efficiency in the Cold Spray Process, *J. Therm. Spray. Technol.,* 1999, **8**(4), p 576-582
22. T.H. Van Steenkiste, J.R. Smith, and R.E. Teets, Aluminum Coatings Via Kinetic Spray with Relatively Large Powder Particles, *Surf. Coat. Technol.,* 2002, **154**(2-3), p 237-252
23. C.-J. Li and W.-Y. Li, Deposition Characteristics of Titanium Coating in Cold Spraying, *Surf. Coat. Technol.,* 2003, **167**(2-3), p 278-283
24. M. Karimi, G.W. Rankin, and A. Fartaj, A Numerical Investigation of the Flowfield of a Supersonic Jet Impinging on a Flat Plate, *Proc. 13th Annual Conference of the CFD Society of Canada* (St. Johns, Newfoundland, Canada), July 13 to Aug 3, 2005, P. Liu, Ed., CFD Society of Canada, 2005, p 231-237
25. Matlab Documentation, The MathWorks Inc., www.mathworks.com, 2005